Rapid Communications | Editors' Suggestion

Coherent long-range transfer of angular momentum between magnon Kittel modes by phonons

K. An,[1] A. N. Litvinenko,[1] R. Kohno,[1] A. A. Fuad,[1] V. V. Naletov,[1,2] L. Vila,[1] U. Ebels,[1] G. de Loubens,[3] H. Hurdequint,[3] N. Beaulieu,[4] J. Ben Youssef,[4] N. Vukadinovic,[5] G. E. W. Bauer,[6] A. N. Slavin,[7] V. S. Tiberkevich,[7] and O. Klein[1,*]

[1]*Université Grenoble Alpes, CEA, CNRS, Grenoble INP, Spintec, 38054 Grenoble, France*
[2]*Institute of Physics, Kazan Federal University, Kazan 420008, Russian Federation*
[3]*SPEC, CEA-Saclay, CNRS, Université Paris-Saclay, 91191 Gif-sur-Yvette, France*
[4]*LabSTICC, CNRS, Université de Bretagne Occidentale, 29238 Brest, France*
[5]*Dassault Aviation, 92552 Saint-Cloud, France*
[6]*Institute for Materials Research and WPI-AIMR and CSRN, Tohoku University, Sendai 980-8577, Japan*
[7]*Department of Physics, Oakland University, Michigan 48309, USA*

(Received 23 May 2019; revised manuscript received 18 September 2019; accepted 14 January 2020; published 21 February 2020)

We report ferromagnetic resonance in the normal configuration of an electrically insulating magnetic bilayer consisting of two yttrium iron garnet (YIG) films epitaxially grown on both sides of a 0.5-mm-thick nonmagnetic gadolinium gallium garnet (GGG) slab. An interference pattern is observed and it is explained as the strong coupling of the magnetization dynamics of the two YIG layers either in phase or out of phase by the standing transverse sound waves, which are excited through a magnetoelastic interaction. This coherent mediation of angular momentum by circularly polarized phonons through a nonmagnetic material over macroscopic distances can be useful for future information technologies.

DOI: 10.1103/PhysRevB.101.060407

The renewed interest in using acoustic oscillators as coherent signal transducers [1–3] stems from the extreme finesse of acoustic signal transmission lines. The low sound attenuation factor η_a benefits the interconversion process into other wave forms (with damping η_s) as measured by the cooperativity $\mathscr{C} = \Omega^2/(2\eta_a\eta_s)$ [4,5], leading to strong coupling as defined by $\mathscr{C} > 1$ even when the coupling strength Ω is small. Here, we present experimental evidence for coherent long-distance transport of angular momentum via the coupling to circularly polarized sound waves that exceeds previous benchmarks set by magnon diffusion [6–8] by orders of magnitude.

The material of choice for magnonics is yttrium iron garnet (YIG) with the lowest magnetic damping reported so far [9,10]. The ultrasonic attenuation coefficient in garnets is also exceptional, i.e., up to an order of magnitude lower than that in single-crystalline quartz [11,12]. Spin waves (magnons) hybridize with lattice vibrations (phonons) by the magnetic anisotropy and strain dependence of the magnetocrystalline energy [13–18]. Although often weak in absolute terms, the magnetoelasticity leads to new hybrid quasiparticles ("magnon polarons") when spin-wave (SW) and acoustic-wave (AW) dispersions (anti)cross [19–21]. This coupling has been exploited in the past to produce microwave acoustic transducers [22,23], parametric acoustic oscillators [24], or nonreciprocal acoustic-wave rotation [25,26]. Recent studies have identified their beneficial effects on spin transport in thin YIG films by pump-and-probe Kerr microscopy [27,28] and in the spin Seebeck effect [29]. The adiabatic conversion between magnons and phonons in magnetic field gradients proves their strong coupling in YIG [30].

But phonons excited by magnetization dynamics can also transfer their angular momentum into an adjacent nonmagnetic dielectrics [32,33]. When the latter acts as a phonon sink, the "phonon pumping" increases the magnetic damping [34]. The substrate of choice for YIG is single-crystal gadolinium gallium garnet (GGG) which in itself has a very long phonon mean free path [35,36] and a small impedance mismatch with YIG [37], raising the hope of a phonon-mediated dynamic exchange of coherence through a nonmagnetic insulating layer [34].

Here, we report ferromagnetic resonance experiments (FMR) of a "dielectric spin-valve" stack consisting of a 0.5-mm-thick single-crystal GGG slab coated on both sides by thin YIG films. We demonstrate that GGG can be an excellent conductor of phononic angular momentum currents allowing the coherent coupling between the two magnets over millimeter distance. Figure 1(a) illustrates the experimental setup in which an inductive antenna monitors the coherent part of the magnetization dynamics. The spectroscopic signature of the dynamic coupling between the two YIG layers is a resonant contrast pattern as a function of microwave frequency [see the intensity modulation along FMR2 in Fig. 1(e)].

Before turning to the experimental details, we sketch a simple phenomenological model that captures the dynamics of the fields as described by the continuum model for magnetoelasticity with proper boundary conditions [34]. The perpendicular dynamics of a trilayer with in-plane translational symmetry can be mapped on three coupled harmonic oscillators, viz., the Kittel modes of the two magnetic layers $m_{i=1,2}$ and the nth mechanical mode u_n in the dielectric, which

*Corresponding author: oklein@cea.fr

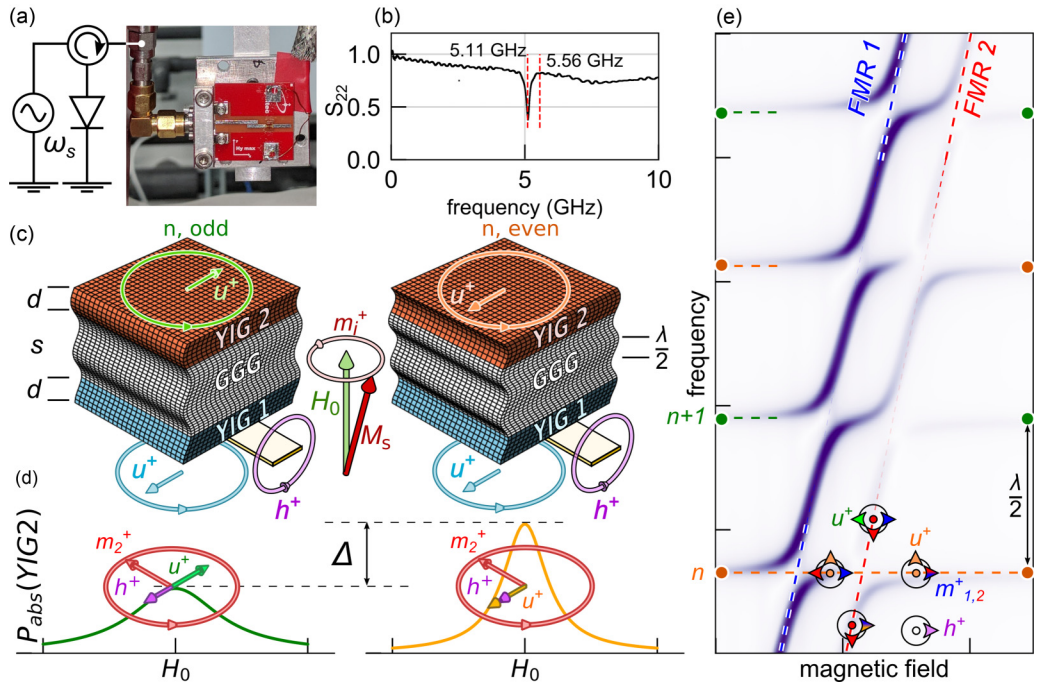

FIG. 1. (a) Schematic and picture of the ferromagnetic resonance (FMR) setup. A butterfly-shaped stripline resonator [31] with 0.3-mm-wide constriction is in contact with the bottom layer of the YIG1($d = 200$ nm)|GGG($s = 0.5$ mm)|YIG2($d = 200$ nm) "dielectric spin-valve" stack. The microwave antenna can be tuned in or out of its fundamental resonance (5.11 GHz) as shown in the reflectivity spectrum (b). (c) Schematic of the coupling between the top (red) and bottom (blue) YIG layers by the exchange of coherent phonons: The magnetic precession m^+ generates a circular shear deformation u^+ of the lattice that can be tuned into a coherent motion of all fields. Constructive/destructive interference between the dynamics of the two YIG layers occurs for even/odd mode numbers n causing (d) a contrast Δ in the absorbed microwave power ($P_{\rm abs}$) between tones separated by half a phonon wavelength. (e) Density plot of the spectral modulation of $P_{\rm abs}$ produced by Eq. (1) when magnetic bilayers are strongly coupled to coherent phonon modes. The orange/green dots indicate the spectral position of the even/odd acoustic resonances.

obey the coupled set of equations

$$(\omega_s - \omega_1 + j\eta_s)m_1^+ = \Omega_1 u_n^+/2 + \kappa_1 h^+, \tag{1a}$$

$$(\omega_s - \omega_2 + j\eta_s)m_2^+ = \Omega_2 u_n^+/2 + \kappa_2 h^+, \tag{1b}$$

$$(\omega_s - \omega_n + j\eta_a)u_n^+ = \Omega_1 m_1^+/2 + \Omega_2 m_2^+/2. \tag{1c}$$

Here, $\omega_n/(2\pi) = v/\lambda_n$, where v is the AW velocity and $\lambda_n/2 = (2d + s)/n$ is a half wavelength that fits into the total sample thickness $2d + s$, with n being an integer (mode number). The dynamic quantities $m_i^+ = (m_x + jm_y)_i$ are circularly polarized magnetic complex amplitudes (j being the imaginary unit) precessing anticlockwise around the equilibrium magnetization at Kittel resonance frequencies $\omega_1 \neq \omega_2$. In our notation $\eta_{s/a}$ are the magnetic/acoustic relaxation rates [38] and the constants Ω_i and κ_i are the magnetoelastic interaction and inductive coupling to the antenna, respectively. Coherence effects between m_1 and m_2 can be monitored by the power $P_{\rm abs} = \kappa_i\,{\rm Im}(h^\star m_i)$ as a function of the microwave frequency ω_s of the driving field with circular amplitude h^+ [39]. Note that Eq. (1) holds when the characteristic AW decay length exceeds the film thickness (see below).

The acoustic modes with odd and even symmetry couple with opposite signs, i.e., $\Omega_2 = (-1)^n\Omega_1$ [see Fig. 1(c)], which affects the dynamics as sketched in Fig. 1(d). When n is odd (even), the top layer returns (absorbs) the power from the electromagnetic field, because the phonon amplitude is out of (in) phase with the direct excitation, corresponding to destructive (constructive) interference. In other words, the phonons pumped by the dynamics of layer 1 are reflected versus absorbed by layer 2. According to Eq. (1), a contrast Δ should emerge between tones separated by half a wavelength. This is illustrated in Fig. 1(e) by plotting the calculated modulation of the magnetic absorption when two Kittel modes with slightly different resonance frequencies and different inductive couplings to the antenna interact via strong coupling to coherent phonons (see below values in Table I). In the figure the effect is more visible around the resonance of the layer with weaker coupling $\kappa_2 < \kappa_1$ to the antenna (FMR2, red dashed line) since, according to the model, the amplitude of the contrast is proportional to the amplitude ratio of the microwave magnetic fields felt by the two YIG layers, $\Delta \propto \kappa_1/\kappa_2$. We employ here a stripline with width (0.3 mm) that couples strongly to the lower layer YIG1, while still allowing to monitor the FMR absorption of YIG2 [40].

TABLE I. Material parameters used in the oscillator model (all values are expressed in units of $2\pi \times 10^6$ rad/s).

$\omega_1 - \omega_2$	$\omega_{n+1} - \omega_n$	Ω	η_s	η_a
40	3.50	1.0	0.50	0.35

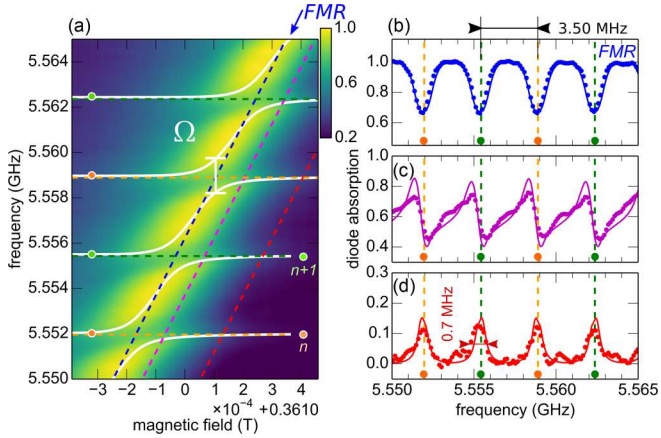

FIG. 2. (a) Microwave absorption spectra of a YIG(200 nm)|GGG(0.5 mm) crystal, revealing a periodic modulation of the intensity interpreted as the avoided crossing between the FMR mode (see blue arrow) at $\omega_1 = \gamma\mu_0(H_0 - M_1)$, and the nth standing (shear) AW_n resonances across the total thickness (horizontal dashed lines in orange and green) at $\omega_n = n\pi v/(d+s)$. The right panels [(b)–(d)] show the intensity modulation for three different cuts (blue, magenta, and red) along the gyromagnetic ratio (i.e., parallel to the resonance condition). The solid lines in the four panels are fits by the oscillator model [cf. Eq. (1) with fit values in Table I].

Figure 1(a) is a picture of the bowtie $\lambda/2$ resonator [with the reflectivity spectrum shown in Fig. 1(b)] with which we perform spectroscopy around 5 GHz. The later fulfills the "half-wave condition" of the phonon relative to the YIG thickness that maximizes the phonon pumping [34]. The sample was grown by liquid phase epitaxy, i.e., by immersing a GGG monocrystal substrate with thickness $s = 0.5$ mm and orientation (111) into molten YIG. The concomitant growth leads to nominally identical YIG layers, with thickness $d = 200$ nm on both sides of the GGG. The Gilbert damping parameter $\alpha \approx 9 \times 10^{-5}$, measured as the slope of the frequency dependence of the linewidth, is evidence of the high crystal quality. All experiments have been carried out at room temperature and on the same sample. Because of that, the results shall be presented in inverse chronological order.

Having removed YIG2 by mechanical polishing, we first concentrate on the dynamic behavior of a single magnetic layer. Figure 2(a) shows the FMR absorption of YIG1|GGG bilayer [41–44] around 5.56 GHz i.e., for a detuned antenna having weak inductive coupling. These spectra are acquired in the perpendicular configuration, where the magnetic precession is circular, by magnetizing the sample with a sufficiently strong external magnetic field H_0 applied along the normal of the films. Figure 2(a) provides a detailed view of the fine structure within the FMR absorption that is obtained when one sweeps the field/frequency in tiny steps of 0.01 mT/0.1 MHz, respectively.

The FMR mode (see arrow) follows the Kittel equation $\omega_1 \approx \gamma\mu_0(H_0 - M_1)$ [45], with $\gamma/(2\pi) = 28.5$ GHz/T the gyromagnetic ratio and $\mu_0 M_1 = 0.1720$ T the saturation magnetization, but its intensity versus frequency is periodically modulated [42,46] which we explain by the hybridization with the comb of standing shear AWs described by Eq. (1) truncated to one magnetic layer.

We ascribe the periodicity of 3.50 MHz in the signal of Fig. 2 to the equidistant splitting of standing phonon modes governed by the *transverse* sound velocity of GGG along (111) of $v = 3.53 \times 10^3$ m/s [42,46,47] via $v/(2d + 2s) \approx 3.53$ MHz [48]. This value thus separates two phononic tones, which differ by half a wavelength. At 5.5 GHz, the intercept between the transverse AW and SW dispersion relations occurs at $2\pi/\lambda_n = \omega_s/v \approx 10^5$ cm^{-1}, which corresponds to a phonon wavelength of about $\lambda_n \approx 700$ nm with index number $n \sim 1400$. The modulation is strong evidence of the high acoustic quality that allows elastic waves to propagate coherently with a decay length exceeding twice the film thickness, i.e., 1 mm. For later reference we point out that the absorption is the same for odd and even phonon modes, whose eigenvalues are indicated here by green and orange dots.

In Figs. 2(b)–2(d) we focus on the line shapes at detunings parallel to the FMR resonance as a function of field and frequency indicated by the blue, magenta, and red cuts in Fig. 2(a). The amplitude of the main resonance (blue line) in Fig. 2(b) dips and the lines broaden at the phonon frequencies [42,46]. The minima transform via a dispersive-looking signal [magenta in Figs. 2(a) and 2(c)] into peaks [red, Figs. 2(a) and 2(d)] once sufficiently far from the Kittel resonance, as expected from the complex impedance of two detuned resonant circuits, illustrating a constant phase between m_i and u_n along these cuts. The m_i are circularly polarized fields rotating in the gyromagnetic direction, that interact only with acoustic waves u_n with the same polarity, as implemented in Eq. (1) [30].

The observed line shapes can be used to extract the lifetime parameters in Eq. (1). We first concentrate on the observed 0.7-MHz full linewidth of the acoustic resonances in Fig. 2(d). Far from the Kittel condition, the absorbed power is governed by the sound attenuation. According to Eq. (1), the absorbed power at large detuning reduces to $P_{\rm abs} \propto [(\omega_s - \omega_n)^2 + \eta_a^2]^{-1}$. The AW decay rate $\eta_a/(2\pi) = 0.35$ MHz is obtained as the half linewidth of the acoustic resonance, leading to a characteristic decay length $\delta = v/\eta_a \approx 2$ mm for AW excited around 5.5 GHz. The acoustic amplitude therefore decays by ~20% over the 0.5-mm film thickness. The sound amplitudes in both magnetic layers are therefore roughly the same, as assumed in Eq. (1). This figure is consistent with the measured ultrasonic attenuation in GGG, 0.70 dB/μs at 1 GHz [36,49], i.e., a lifetime of about 0.5 μs at 5 GHz.

The SW lifetime $1/\eta_s$ follows from the broadening of the absorbed power at the Kittel condition which contains a constant inhomogeneous contribution and a frequency-dependent viscous damping term. When plotted as a function of frequency, the former is the extrapolation of the linewidths to zero frequency, in our case ~5.7 MHz (or 0.2 mT). On the other hand, the Gilbert phenomenology (see above) of the homogeneous broadening $\eta_s = \alpha\omega_s$ corresponds to a $\eta_s/(2\pi) = 0.50$ MHz at 5.5 GHz. The dominantly inhomogeneous broadening is here caused by thickness variations, a spatially dependent magnetic anisotropy, but also by the inhomogeneous microwave field.

Conspicuous features in Fig. 2(a) are the clearly resolved avoided crossings of SW and AW dispersion relations, which

prove the strong coupling between two oscillators. Fitting by hand the dispersions of two coupled oscillators through the data points (white lines), we extract a gap of $\Omega/(2\pi) = 1$ MHz and a large cooperativity $\mathscr{C} \approx 3$. From the overlap integral between a standing shear AW confined in a layer of thickness s and the Kittel mode confined in a layer of thickness d, one can derive the analytical expression for the magnetoelastic coupling strength [42,50],

$$\Omega = \frac{B}{\sqrt{2}}\sqrt{\frac{\gamma}{\omega_s M_1 \rho s d}}\left(1 - \cos\omega_s \frac{d}{v}\right), \tag{2}$$

where [35] $B = (B_2 + 2B_1)/3 = 7 \times 10^5$ J/m^3, with B_1 and B_2 being the magnetoelastic coupling constants for a cubic crystal, and $\rho = 5.1$ g/cm^3 is the mass density of YIG. From Eq. (2) we infer that coherent SW excited around $\omega_s/(2\pi) \approx 5.5$ GHz have a dynamic coupling to shear AW of the order of $\Omega/(2\pi) = 1.5$ MHz, close to the value extracted from the experiments.

The material parameters extracted for our YIG|GGG are summarized in Table I. Numerical solutions of Eq. (1) using these values are shown as solid lines in Figs. 2(b)–2(d). The agreement with the data is excellent, confirming the validity of the model and parameters.

The other needed parameter for solving Eq. (1) in the general case is the attenuation ratio $\kappa_2/\kappa_1 \approx 7$ deducted from a factor of 50 decreased power when flipping the single YIG layer sample upside down on the antenna. The layer is then separated 0.5 mm from the antenna, and the observed reduction agrees with numerical simulations using electromagnetic field solvers.

We turn now our attention to the magnetic sandwich in which YIG1 touches the antenna and the nominally identical YIG2 is 0.5 mm away, where a slight difference in uniaxial anisotropy causes separate resonance frequencies. Since we want to detect also the resonance of the top layer, we have to compensate for the decrease in inductive coupling by tuning the source frequency to the antenna resonance at 5.11 GHz [see Fig. 1(b)]. This enhances the signal by the quality factor $Q \sim 30$ of the cavity at the cost of an increased radiative damping of the bottom layer signal [51].

Figure 3(a) is a transparent overlay of field sweeps for frequency steps of 0.1 MHz in the interval 5.101 ± 0.008 GHz. We attribute the two peaks separated by 1.4 mT (or 40 MHz) to the bottom and top YIG Kittel resonances, the latter shifted due to a slight difference in effective magnetization $\mu_0 M_2 = \mu_0 M_1 + 0.0014$ T. Note that the detuning between the two Kittel modes is large compared to the strength of the magnetoelastic coupling Ω. In Figs. 3(b) and 3(c) we compare the measured modulation of the resonance amplitude for respectively the bottom YIG1 layer and top YIG2 layers. This corresponds to performing two cuts at the resonance condition FMR1 and FMR2 in the same fashion as Fig. 2(b). The top YIG2 signal is modulated with a period of 7.00 MHz [Fig. 3(c)] with a contrast Δ between even and odd modes. This agrees with the prediction of Eq. (1) (see solid lines) due to constructive/destructive couplings mediated by even/odd phonon modes, the modulation period of the absorbed power doubles along the resonance of the top layer (FMR2), when compared to the case of a single YIG layer (Fig. 2).

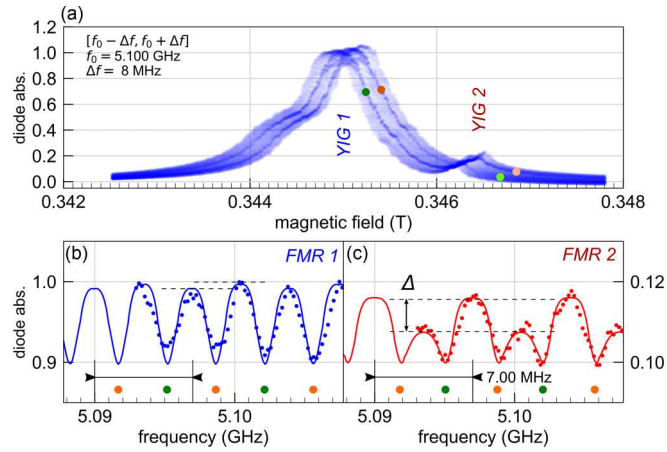

FIG. 3. FMR spectroscopy of the YIG1|GGG|YIG2 trilayer. (a) is a transparent overlay of magnetic field sweeps for frequencies in the interval 5.101 ± 0.008 GHz by 0.1-MHz steps. Dark lines reveal two acoustic resonances marked by orange and green dots. (b) and (c) show the frequency modulation of the FMR amplitude for respectively the bottom YIG1 layer and the top YIG2 layer, in which a contrast Δ appears between neighboring acoustic resonances. The solid lines show the modulation predicted by Eq. (1).

Figure 3(b) illustrates also that the strong coupling κ_1 to the antenna hinders a clear observation of this modulation in the bottom YIG1 layer resonance. Nevertheless, the anticipated sign change of Δ [by the inverted phase of u_n relative to m_2 in Eq. (1)] between FMR1 and FMR2 remains observable.

We now address the acoustic resonances revealed by the dark lines in Fig. 3(a) for odd/even indices labeled by green/orange circles in the wings. The phonon line with an even index (orange marker) progressively disappears when approaching the YIG2 Kittel resonance from the low field (left side) of the resonance, while the opposite behavior is observed for the odd index feature (green marker), which disappears when approaching the YIG2 Kittel resonance from the high field (right side). This behavior agrees with the model in Fig. 1(e). The contrast in the acoustic resonance intensity mirrors the contrast of the amplitude of the FMR resonance.

Figure 4(a) shows the observed FMR absorption spectrum around 5.11 GHz measured at a fixed field $H_0 = 0.3453$ T. We enhance the fine structure in Fig. 4(b) by subtracting the FMR envelope and progressively amplifying the weak signals in the wings. The orange/green color code emphasizes the constructive/destructive interference of the even/odd acoustic resonances in the top-layer signal. This feature can be explained by Eq. (1), as shown by the calculated curves in Figs. 4(c) and 4(d). The acoustic modes change character from even to odd (or vice versa) across the FMR frequency, which is caused by the associated phase shift by 180° of the acoustic drive, again explaining the experiments. The absorption by the YIG2 top layer in Fig. 4(d) may even become negative so the phonon current from YIG1 drives the magnetization in YIG2. This establishes both angular momentum and power transfer of microwave radiation via phonons.

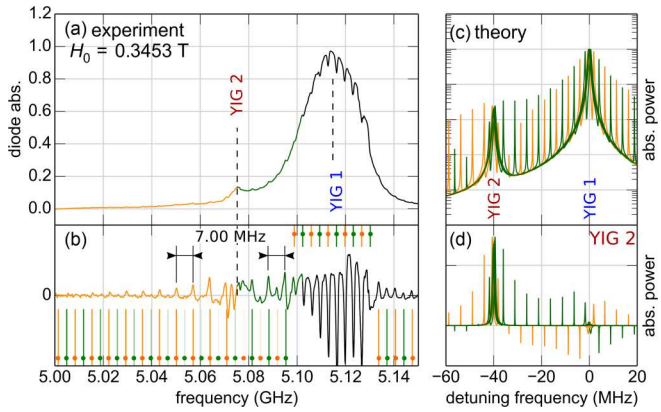

FIG. 4. (a) Frequency sweep at fixed field performed on the magnetic bilayer. The fine regular modulation within the FMR envelope is ascribed to the excitation of acoustic shear wave resonances. The acoustic pattern is enhanced in (b) by subtracting the FMR envelope emphasizing the constructive/destructive interferences of the even/odd acoustic resonances in the vicinity of the YIG2 FMR mode. (c) shows on a logarithmic scale the predicted modulation using the experimental parameters of Table I. (d) shows on a linear scale the corresponding power absorbed by the top magnetic layer only.

In summary, we report interferences between the Kittel resonances of two ferromagnets over a macroscopic distance through the exchange of circularly polarized coherent shear waves propagating in a nonmagnetic dielectric. We show that magnets are a source and detector for phononic angular momentum currents and that these currents provide a coupling, analogous to the dynamic coupling in metallic spin valves [52], but with an insulating spacer, over much larger distances, and in the ballistic/coherent rather than diffuse/dissipative regime. This should lead to the creation of a dynamical gap between the collective states when the two Kittel resonances are tuned within the strength of the magnetoelastic coupling. Our findings might have implications on the nonlocal spin transport experiments [53], in which phonons provide a parallel channel for the transport of angular momentum. While the present experiments are carried out at room temperature and interpreted classically, the high acoustic quality of phonon transport and the strong coupling to the magnetic order in insulators may be useful for quantum communication.

This work was supported in part by Grant No. 18-CE24-0021 from the ANR of France, Grants No. EFMA-1641989 and No. ECCS-1708982 from the U.S. NSF, by the Oakland University Foundation, the NWO, and Grants-in-Aid of the Japan Society of the Promotion of Science (Grant No. 19H006450). V.V.N. acknowledges support from UGA through the invited professor program and from the Russian Competitive Growth of KFU. We would like to thank Simon Streib for illuminating discussions.

[1] A. Bienfait, K. J. Satzinger, Y. P. Zhong, H.-S. Chang, M.-H. Chou, C. R. Conner, É. Dumur, J. Grebel, G. A. Peairs, R. G. Povey, and A. N. Cleland, Science **364**, 368 (2019).
[2] B. A. Moores, L. R. Sletten, J. J. Viennot, and K. W. Lehnert, Phys. Rev. Lett. **120**, 227701 (2018).
[3] Y. Tsaturyan, A. Barg, E. S. Polzik, and A. Schliesser, Nat. Nanotechnol. **12**, 776 (2017).
[4] S. Al-Sumaidae, M. H. Bitarafan, C. A. Potts, J. P. Davis, and R. G. DeCorby, Opt. Express **26**, 11201 (2018).
[5] N. Spethmann, J. Kohler, S. Schreppler, L. Buchmann, and D. M. Stamper-Kurn, Nat. Phys. **12**, 27 (2015).
[6] L. J. Cornelissen, J. Liu, R. A. Duine, J. B. Youssef, and B. J. van Wees, Nat. Phys. **11**, 1022 (2015).
[7] K. Oyanagi, S. Takahashi, L. J. Cornelissen, J. Shan, S. Daimon, T. Kikkawa, G. E. W. Bauer, B. J. van Wees, and E. Saitoh, Nat. Commun. **10**, 4740 (2019).
[8] R. Lebrun, A. Ross, S. A. Bender, A. Qaiumzadeh, L. Baldrati, J. Cramer, A. Brataas, R. A. Duine, and M. Klui, Nature (London) **561**, 222 (2018).
[9] E. G. Spencer, R. C. LeCraw, and A. M. Clogston, Phys. Rev. Lett. **3**, 32 (1959).
[10] V. Cherepanov, I. Kolokolov, and V. L'vov, Phys. Rep. **229**, 81 (1993).
[11] R. LeCraw and R. Comstock, in *Physical Acoustics*, Vol. 3 (Elsevier, Amsterdam, 1965), pp. 127–199.
[12] E. G. Spencer, R. T. Denton, and R. P. Chambers, Phys. Rev. **125**, 1950 (1962).
[13] C. Kittel, Phys. Rev. **110**, 836 (1958).
[14] H. Bmmel and K. Dransfeld, Phys. Rev. Lett. **3**, 83 (1959).
[15] R. Damon and H. van de Vaart, Proc. IEEE **53**, 348 (1965).
[16] M. Seavey, Proc. IEEE **53**, 1387 (1965).
[17] L. Dreher, M. Weiler, M. Pernpeintner, H. Huebl, R. Gross, M. S. Brandt, and S. T. B. Goennenwein, Phys. Rev. B **86**, 134415 (2012).
[18] X. Zhang, C.-L. Zou, L. Jiang, and H. X. Tang, Sci. Adv. **2**, e1501286 (2016).
[19] A. G. Gurevich and G. A. Melkov, *Magnetization Oscillations and Waves* (CRC Press, Boca Raton, FL, 1996).
[20] H. Dötsch, P. Röschmann, and W. Schilz, Appl. Phys. **15**, 167 (1978).
[21] K. Wago, D. Botkin, C. S. Yannoni, and D. Rugar, Appl. Phys. Lett. **72**, 2757 (1998).
[22] M. Pomerantz, Phys. Rev. Lett. **7**, 312 (1961).
[23] T. Reeder and D. Winslow, IEEE Trans. Microwave Theory Tech. **17**, 927 (1969).
[24] P. Chowdhury, P. Dhagat, and A. Jander, IEEE Trans. Magn. **51**, 1 (2015).
[25] B.-I. Popa and S. A. Cummer, Nat. Commun. **5**, 3398 (2014).
[26] H. Matthews and R. C. LeCraw, Phys. Rev. Lett. **8**, 397 (1962).
[27] N. Ogawa, W. Koshibae, A. J. Beekman, N. Nagaosa, M. Kubota, M. Kawasaki, and Y. Tokura, Proc. Natl. Acad. Sci. USA **112**, 8977 (2015).
[28] Y. Hashimoto, S. Daimon, R. Iguchi, Y. Oikawa, K. Shen, K. Sato, D. Bossini, Y. Tabuchi, T. Satoh, B. Hillebrands, G. E. W. Bauer, T. H. Johansen, A. Kirilyuk, T. Rasing, and E. Saitoh, Nat. Commun. **8**, 15859 (2017).

[29] T. Kikkawa, K. Shen, B. Flebus, R. A. Duine, K.-i. Uchida, Z. Qiu, G. E. W. Bauer, and E. Saitoh, Phys. Rev. Lett. **117**, 207203 (2016).
[30] J. Holanda, D. S. Maior, A. Azevedo, and S. M. Rezende, Nat. Phys. **14**, 500 (2018).
[31] Y. S. Yap, H. Yamamoto, Y. Tabuchi, M. Negoro, A. Kagawa, and M. Kitagawa, J. Magn. Reson. **232**, 62 (2013).
[32] R. L. Comstock and R. C. LeCraw, J. Appl. Phys. **34**, 3022 (1963).
[33] D. A. Garanin and E. M. Chudnovsky, Phys. Rev. B **92**, 024421 (2015).
[34] S. Streib, H. Keshtgar, and G. E. W. Bauer, Phys. Rev. Lett. **121**, 027202 (2018).
[35] E. G. Spencer, R. T. Denton, T. B. Bateman, W. B. Snow, and L. G. V. Uitert, J. Appl. Phys. **34**, 3059 (1963).
[36] M. Dutoit and D. Bellavance, in *1972 Ultrasonics Symposium* (IEEE, New York, 1972).
[37] N. Polzikova, S. Alekseev, V. Luzanov, and A. Raevskiy, J. Magn. Magn. Mater. **479**, 38 (2019).
[38] A. Rückriegel, P. Kopietz, D. A. Bozhko, A. A. Serga, and B. Hillebrands, Phys. Rev. B **89**, 184413 (2014).
[39] The antenna produces a linear rf field, which decomposes in both a left and right circulating field with only one component coupling to the magnetization dynamics.
[40] We disregard the inhomogeneity in the driving field generated by the local antenna.
[41] Y. V. Gulyaev, P. E. Zil'berman, G. T. Kazakov, V. G. Sysoev, V. V. Tikhonov, Y. A. Filimonov, B. P. Nam, and A. S. Khe, JETP Lett. **34**, 500 (1981).
[42] M. Ye, A. Brockmeyer, P. E. Wigen, and H. Dötsch, J. Phys. Colloq. **49**, C8 (1988).
[43] A. N. Litvinenko, A. V. Sadovnikov, V. V. Tikhonov, and S. A. Nikitov, IEEE Magn. Lett. **6**, 1 (2015).
[44] V. V. Tikhonov and S. A. Nikitov, Bull. Russ. Acad. Sci.: Phys. **81**, 969 (2017).
[45] The exact expression is more complicated and contains cubic/uniaxial anisotropies of $H_{k1} = -7.8$ mT/$H_{ku} = -3.75$ mT, respectively.
[46] M. Ye and H. Dötsch, Phys. Rev. B **44**, 9458 (1991).
[47] Y. V. Khivintsev, V. K. Sakharov, S. L. Vysotskii, Y. A. Filimonov, A. I. Stognii, and S. A. Nikitov, Tech. Phys. **63**, 1029 (2018).
[48] The total crystal thickness reduces to $d + s$ after polishing.
[49] M. Dutoit, J. Appl. Phys. **45**, 2836 (1974).
[50] R. S. Khymyn, V. S. Tiberkevich, and A. N. Slavin (unpublished).
[51] N. Bloembergen and R. V. Pound, Phys. Rev. **95**, 8 (1954).
[52] B. Heinrich, Y. Tserkovnyak, G. Woltersdorf, A. Brataas, R. Urban, and G. E. W. Bauer, Phys. Rev. Lett. **90**, 187601 (2003).
[53] L. J. Cornelissen, K. Oyanagi, T. Kikkawa, Z. Qiu, T. Kuschel, G. E. W. Bauer, B. J. van Wees, and E. Saitoh, Phys. Rev. B **96**, 104441 (2017).